Threshold behavior of the Einstein oscillator, electron-phonon interaction, band-edge absorption, and small hole polarons in $LiNbO_3$:Mg crystals

Feifei Xin, Zhaohui Zhai, Xiaojie Wang, Yongfa Kong, Jingjun Xu, and Guoquan Zhang*

The MOE Key Laboratory of Weak Light Nonlinear Photonics, School of Physics and TEDA Applied Physics School, Nankai University, Tianjin 300457, China

(Received 19 December 2011; revised manuscript received 22 July 2012; published 24 October 2012)

Based on the Einstein oscillator model and the Urbach rule, we study the electron-phonon interaction and the band-edge structure of $LiNbO_3$:Mg. We report on the concentration threshold behavior of the Einstein oscillator, the electron-phonon interaction, the band-edge absorption, and the light-induced small hole polarons O^- in $LiNbO_3$:Mg crystals with increasing Mg-doping concentration. The result gives a fundamental microscopic mechanism of the concentration threshold behavior related to the band-edge optical properties and the light-induced charge transport of $LiNbO_3$:Mg crystals, and is helpful to optimize $LiNbO_3$ for applications such as nonlinear optics.

DOI: 10.1103/PhysRevB.86.165132 PACS number(s): 78.40.−q, 42.70.Gi, 71.38.Ht, 78.20.Mg

Lithium niobate ($LiNbO_3$) is a versatile synthetic crystal because of its good electro-optic, acousto-optic, elasto-optic, pyroelectric, and nonlinear optic properties, and has numerous potential applications in holographic storage, laser physics, information processing, and nonlinear optics.[1] It is well demonstrated that $LiNbO_3$ can be modified for a specific application by controlling the extrinsic and intrinsic defect structures in crystal through doping and composition modification.[1–8] Specifically, the optical damage in the visible and near infrared is significantly suppressed in highly doped $LiNbO_3$:Mg, showing a Mg-doping concentration threshold behavior.[2,3] On the contrary, the threshold behavior in the ultraviolet (UV) is opposite to that in the visible and near infrared, and the photorefractivity and the light-induced absorption change in highly doped $LiNbO_3$:Mg are greatly enhanced in the UV.[6–8] The threshold behavior in the visible and near infrared is phenomenologically ascribed to the increase of photoconductivity due to the disappearance of antisite Nb_{Li}^{5+} defect in highly doped $LiNbO_3$:Mg[3], while the mechanism for the opposite threshold behavior in the UV is not clear up to now. More importantly, a systematic study on the electron-phonon interaction and band-edge structure of $LiNbO_3$, which determine a broad range of properties related to optics, electron, and thermal transport,[9] is still lacking.

In this paper, we report on the Mg-doping concentration threshold behavior of the Einstein oscillator, the electron-phonon interaction, and the band-edge absorption of $LiNbO_3$:Mg. A broad band-edge absorption band is observed in $LiNbO_3$:Mg crystals at cryogenic temperatures. In addition, two different UV-light-induced small hole polarons O^- are identified. These defect structures and the light-induced charge transport determine the optical properties of $LiNbO_3$:Mg in the UV. The result also provides a microscopic picture for the concentration threshold behavior of optical properties of $LiNbO_3$:Mg.

A series of congruent $LiNbO_3$:Mg crystals with a Li/Nb ratio of 0.94 and Mg-doping concentrations of 1.0, 2.0, 3.0, 4.0, 5.0, 6.5, 7.8, and 9.0 mol% MgO in melt were prepared and labeled as CMg1, CMg2, CMg3, CMg4, CMg5, CMg6.5, CMg7.8, and CMg9, respectively. A nominally pure congruent $LiNbO_3$ crystal labeled as CLN was also employed for comparison. The thickness of all samples was 0.5 mm. The UV band-edge absorption spectra in the temperature range from 3.8 to 973 K were measured for all crystals. The spectral dichroism was found to be negligible, therefore, the data presented in this paper is only for the extraordinary polarized light.

The absorption band edge was found to be redshifted significantly with the increase of crystal temperature in all samples; therefore the effective band energy gap E_g, defined as the photon energy at which $\alpha = 70\ \mathrm{cm}^{-1}$, decreases with the increase of temperature, as shown in Fig. 1(a) for CLN, as an example. Here, we could not directly measure the direct band gap due to the limitation of the spectrometer. Instead, we employed the generally accepted definition of the band edge of $LiNbO_3$ by taking the photon energy corresponding to a specific absorption coefficient on the absorption edge (usually at $\alpha = 15$ or $20\ \mathrm{cm}^{-1}$ in the literature[10–12]). In order to avoid the possible influence from the defect structures near the band edge, as we will show below, we took the corresponding photon energy as high as possible, which is limited only by our spectrometer. The temperature dependence of E_g can be well described by the Bose-Einstein expression[13]

$$E_g(T) = E_{gBE}(0) - \frac{2a_B}{\exp(E_{pBE}/k_BT) - 1}, \qquad (1)$$

where T is the absolute temperature, k_B is the Boltzmann constant, $E_{gBE}(0)$ is the fundamental band gap at $T = 0$, E_{pBE} is the average energy of the Einstein oscillator corresponding to the most active phonons,[9] and a_B represents the strength of the electron-phonon interaction. The fitting result for CLN is shown in Fig. 1(a), and excellent fits are also achieved for all other samples. The yielded values of $E_{gBE}(0)$, E_{pBE}, and a_B are shown in Figs. 1(b)–1(d), respectively. It is found that the fundamental band gap $E_{gBE}(0)$ increases up to ∼4.30 eV at around 6.5 mol% Mg-doping concentration, and then it goes down slightly as the Mg-doping concentration continues to grow. Surprisingly but interestingly, the Einstein oscillator and the electron-phonon interaction exhibit a distinct Mg-doping concentration threshold behavior. As shown in Figs. 1(c) and 1(d), the Einstein oscillator energy E_{pBE} drops abruptly from ∼400 cm^{-1} to ∼250 cm^{-1} and the

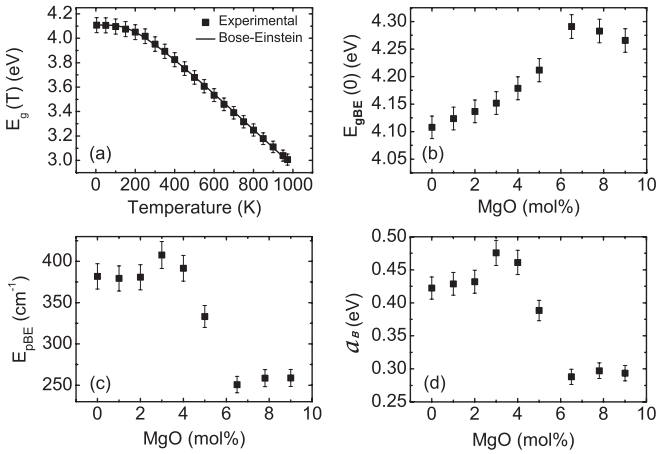

FIG. 1. (a) The measured temperature dependence of the effective band energy gap of CLN and the corresponding fitting curve by the Bose-Einstein expression. The dependence of (b) the fundamental band gap at 0 K, (c) the average energy of the Einstein oscillator, and (d) the strength of the electron-phonon interaction on the Mg-doping concentration, respectively.

electron-phonon interaction strength weakens dramatically at around 5.0 mol% Mg-doping concentration. Note that the electron-phonon interaction determines a broad range of optical properties and the electron transport in crystal. The reduction in the electron-phonon interaction would lead to an increase in the photoconductivity,[9] which finally results in the suppression of optical damage in highly Mg-doped $LiNbO_3$.[2,3] The result, therefore, gives a fundamental microscopic picture of the threshold behavior of optical properties such as the optical damage and spectral properties of $LiNbO_3$:Mg crystals.

The absorption edge tails of all samples at temperatures higher than 400 K are consistent with the widely observed Urbach rule[14–17]

$$\alpha = \alpha_0 \exp\left[\frac{\sigma}{k_B T^*}(\hbar\omega - \hbar\omega_0)\right], \tag{2}$$

where α_0, σ, and ω_0 are constants, and T^* is the effective temperature being determined by

$$T^* = \frac{\hbar\omega_p}{2k_B}\coth\left(\frac{\hbar\omega_p}{2k_B T}\right), \tag{3}$$

and ω_p is the phonon frequency at which the most active interaction occurs with electrons. As an example, Fig. 2(a) shows the semilogarithmic spectral plots of the absorption edge of all samples vs photon energy $E = \hbar\omega$ at 500 K. The energy of the most active phonons $E_{pU} = \hbar\omega_p$ was calculated for all samples by fitting the measured absorption edges using Eqs. (2) and (3), as shown in Fig. 2(b). As expected, the energy E_{pU} also exhibits a Mg-doping concentration threshold behavior, which is exactly the same as that of the Einstein oscillator shown in Fig. 1(c). In fact, the Urbach rule can also be well modeled by the Einstein oscillator.[18,19] For $LiNbO_3$ crystals, the fundamental optical transition occurs in NbO_6 octahedra,[16,20] and the microscopic electric fields associated with the longitudinal optical phonons are primarily responsible for the Urbach rule.[21] The significant drop of the average phonon energy from ~400 cm^{-1} to ~250 cm^{-1} when the Mg-doping concentration exceeds 5.0 mol% reveals a dramatic

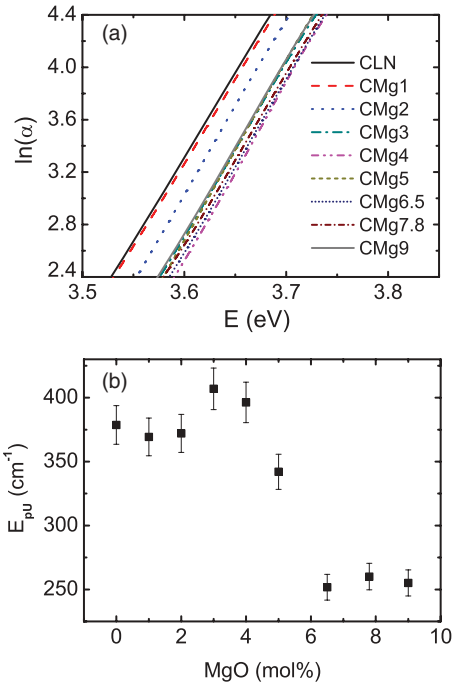

FIG. 2. (Color online) (a) Spectral profiles of ln(α) at 500 K and (b) the energy of the most active phonons $E_{pU} = \hbar\omega_p$ for $LiNbO_3$ with different Mg-doping concentrations.

deformation of the NbO_6 framework,[22] which is in excellent accordance with the defect structure changes of crystals around the threshold concentration of MgO, at which Mg^{2+} ions begin to replace the Nb^{5+} ions in the NbO_6 octahedra.[23]

Interestingly, as the temperature goes down below ~400 K and the absorption edge of the crystal gradually shifts toward higher energy, a new absorption band shows up at the bottom of the Urbach tail in all samples. Typical absorption spectra at a cryogenic temperature of 3.8 K for all samples are shown in Fig. 3. The appearance of this new absorption band deforms the Urbach tail at this spectral region, which may also deviate the effective band energy gap E_g of the crystal if it is defined as the photon energy at which $\alpha = 15$ or 20 cm^{-1}. On the other hand, we found that, although the profile of the absorption edge tail around this new band deviates from the Urbach rule, the remaining part of the absorption edge tail

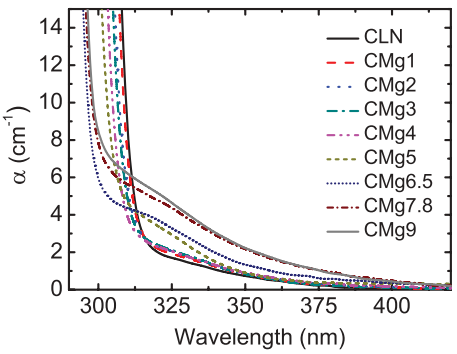

FIG. 3. (Color online) The absorption spectra of $LiNbO_3$:Mg crystals with various doping concentrations at 3.8 K.

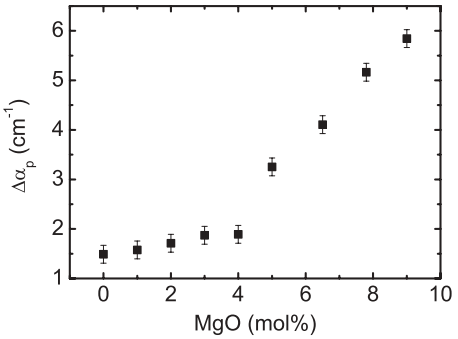

FIG. 4. Dependence of the absorption peak $\Delta\alpha_p$ on the Mg-doping concentration measured at 3.8 K.

still obeys the Urbach rule. In order to show the true spectral structure of this absorption band, we subtract the Urbach tail from the measured spectra and get

$$\Delta\alpha = \alpha - \alpha_0 \exp\left[\frac{\sigma}{k_B T^*}(\hbar\omega - \hbar\omega_0)\right], \tag{4}$$

where α_0, σ, ω_0, and T^* are calculated by fitting the remaining spectrum without deformation to the Urbach rule. We find that the peak of the absorption band $\Delta\alpha_p$ grows with increasing MgO concentration, as shown in Fig. 4. In the lightly doped $LiNbO_3$:Mg (<5.0 mol%), the absorption peak $\Delta\alpha_p$ varies slightly with the increase of Mg-doping concentration, while an abrupt increase of $\Delta\alpha_p$ is observed in the sample CMg5 followed by a significant increase of $\Delta\alpha_p$ as the Mg-doping concentration continues to increase. Note that the increased slope of $\Delta\alpha_p$ for the highly doped region is much steeper than that for the lightly doped region in Fig. 4, indicating the dominant defect centers responsible for $\Delta\alpha$ should be different for the lightly and highly doped $LiNbO_3$:Mg crystals. Note that the UV photorefractivity is enhanced significantly when the Mg-doping concentration is higher than 5.0 mol%,[6,7] which has exactly the same tendency as the strength of the absorption band $\Delta\alpha$ shown in Figs. 3 and 4. This indicates that the related defect centers should also be responsible for the photorefraction and the light-induced charge transport process in the UV in $LiNbO_3$:Mg.

Moreover, for crystals with Mg-doping concentrations higher than 5.0 mol%, the absorption band $\Delta\alpha$ can be decomposed into two Gaussian components peaked at 3.83 and 4.03 eV, respectively. Figure 5(a) shows a typical spectral profile of $\Delta\alpha$ for the sample CMg6.5 measured at 3.8 K, together with the spectral profiles of the two decomposed Gaussian components and their summation. For crystals with Mg-doping concentrations lower than 5.0 mol%, only the Gaussian component peaked at 3.83 eV appears in the spectra of $\Delta\alpha$. A typical result for the case of CLN measured at 3.8 K is shown in Fig. 5(b), where the dash-dotted red curve is a least-square fit of a Gaussian spectral profile with its peak energy fixed at 3.83 eV. It is clear that the defect centers responsible for $\Delta\alpha$ are different in the lightly and highly doped $LiNbO_3$:Mg crystals.

In order to clarify the related defect centers near the band edge, we measured the spectra of the UV-light-induced absorption change of $LiNbO_3$:Mg. The UV pump beam, with an intensity of 0.26 W/cm^2, was set at 325 nm, very

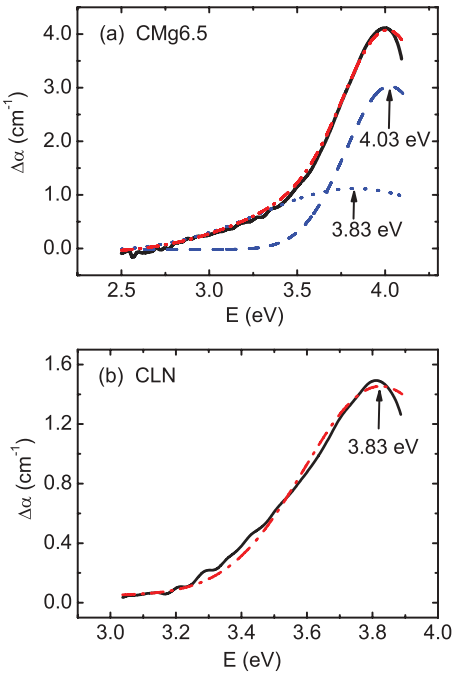

FIG. 5. (Color online) The spectral profiles of $\Delta\alpha$ (black curves) measured at 3.8 K for CMg6.5 (a) and CLN (b), respectively. The dotted and dashed blue curves in (a) are the theoretical fits of two Gaussian components peaked at 3.83 and 4.03 eV, respectively, and the dash-dotted red curve in (a) is the sum of the two Gaussian components. The dash-dotted red curve in (b) is the theoretical fit with a Gaussian profile peaked at 3.83 eV.

close to the absorption peak of $\Delta\alpha$ in Fig. 5. For crystals with low Mg-doping concentrations (<4 mol%, including CLN), no detectable light-induced absorption change was observed, most probably because of the low available UV-pump intensity and the limitation of the detection sensitivity of the spectrometer. For highly Mg-doped crystals ($\geqslant$5 mol%), a broad light-induced absorption spectral band, extending from the visible to the UV, was observed. We may attribute the observed spectrum of the light-induced absorption change $\Delta\alpha_{li}$ to the formation of small hole polarons O^- near the negatively charged defect centers in crystals.[9,24,25]

Figure 6 shows a typical spectrum of the UV-light-induced absorption changes $\Delta\alpha_{li}$ for CMg5 at room temperature (298 K). This broad spectrum of the light-induced absorption change can be well decomposed into two Gaussian-type spectral profiles with typical characteristics of small hole polarons O^-:[24,25]

$$\Delta\alpha_{li} = \sum_{i=1,2} \frac{\Delta\alpha_i}{\hbar\omega} \exp[-w_i(\hbar\omega - M_i)^2], \tag{5}$$

where $\Delta\alpha_i$ and w_i are constants, $M_i = 2E_{pi}$ is the peak spectral energy of the respective small hole polarons, and E_{pi} is the energy of the hole-vibration system under the six-well model.[25,27] The peak energy was measured to be 2.64 and 3.45 eV, and the fingerprint ratio $W^2/M = 2\ln(2)\hbar\omega_0$, where W is the half-width at half-maximum of the polaronic spectrum (see the dashed and dotted blue curves in Fig. 6) and $\hbar\omega_0$ is the typical longitudinal optical phonon energy, was 0.15 and 0.04 eV for the respective small hole polarons. The

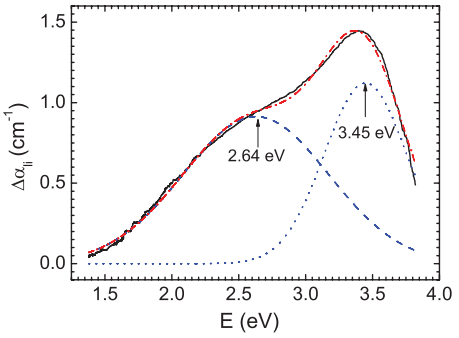

FIG. 6. (Color online) The spectral profile of the UV-light-induced absorption changes $\Delta\alpha_{li}$ measured at room temperature (298 K) for CMg5. The solid black curve is the measured one, and the dashed and dotted blue curves are the theoretical fits of two Gaussian-type polaronic components peaked at 2.64 and 3.45 eV, respectively, and the dash-dotted red curve is the sum of the two Gaussian-type polaronic components according to Eq. (5).

spectral characteristics with a peak energy of 2.64 eV and a fingerprint ratio $W^2/M = 0.15$ eV (see the dashed blue curve in Fig. 6) are in good accordance with those of small hole polaron (O^--V_{Li}), in which a hole is trapped at an oxygen ion near a Li-site vacancy (V_{Li}).[24,25] On the other hand, we may attribute the spectrum with a high peak energy of 3.45 eV and a ratio $W^2/M = 0.04$ eV (see the dotted blue curve in Fig. 6) to the formation of small hole polarons near other negatively charged defect centers, most probably the Mg_{Nb}^{2+} centers.[23] It is well known that, when the Mg-doping concentration is lower than 5.0 mol% in melt, the main negatively charged defect center in $LiNbO_3$:Mg crystal is the Li-site vacancy V_{Li},[23] and the O^- polaron can be formed when a hole is trapped at an oxygen ion near a Li-site vacancy (O^--V_{Li}).[24] When the Mg-doping concentration is higher than 5.0 mol%, Mg^{2+} ions will replace the normal Nb^{5+} ions and form negatively charged (with respect to the normal lattice) centers Mg_{Nb}^{2+},[23] which has a higher electronegativity than V_{Li}. Therefore, holes may also be trapped at oxygen ions near the Mg_{Nb}^{2+} centers, forming another type of O^- polarons (O^--Mg_{Nb}^{2+}) in highly Mg-doped $LiNbO_3$.[26] In addition, we noticed that a broadband but very weak (with a peak amplitude of $\sim$0.08 cm^{-1}) UV-light-induced absorption change spectrum similar to that in Fig. 6 was also observed in CMg4. This indicates that Mg^{2+} ions already begin to replace normal site Nb ions at this Mg-doping concentration.

One may argue that the typical fingerprint ratio W^2/M would be $\sim$0.14 eV for small hole polarons, while that measured for the dotted blue curve in Fig. 6 is only 0.04 eV. This discrepancy may be ascribed to the following reasons: (1) Note that the ratio W^2/M is proportional to the coupled longitudinal phonon energy;[25] a dramatic decrease in the longitudinal phonon energy will reduce the ratio. Such a dramatic decrease in the longitudinal phonon energy was indeed observed in highly Mg-doped $LiNbO_3$, as shown in Figs. 1(c) and 2(b). (2) A reduced coupling strength with the lattice, as shown in Fig. 1(d), would narrow the spectral bandwidth of small hole polarons.[25,27] (3) The Mg_{Nb}^{2+} center is of higher electronegativity as compared to the V_{Li} center, and holes are bounded much more tightly around Mg_{Nb}^{2+} centers, which may result in an increase in the peak energy of the small hole polarons, and therefore reduce the ratio further.

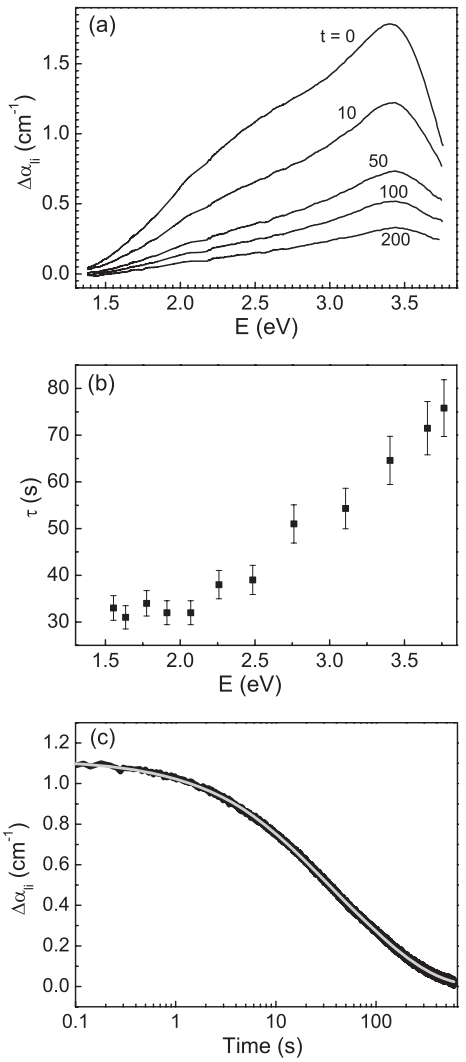

FIG. 7. (a) The spectral profiles of the UV-light-induced absorption changes $\Delta\alpha_{li}$ at specific dark decay times $t = 0$, 10, 50, 100, and 200 s, respectively; (b) the dark decay time constants τ probed at specific wavelengths which are estimated as the time for the UV-light-induced absorption changes decaying to its e^{-1} of its initial value at $t = 0$; and (c) the temporal dark decay dynamics of the UV-light-induced absorption change probed at 400 nm. All the data (solid curves and solid squares) were measured at room temperature (298 K) for CMg5. The gray curve in (c) is the theoretical fit to the sum of two stretched exponential decays according to Eq. (6).

Figure 7(a) shows the typical dark decay dynamics of the UV-light-induced absorption change for CMg5 at room temperature. It is clearly seen that the UV-light-induced absorption spectrum peaked at 2.64 eV decays much faster than that peaked at 3.45 eV. This was further confirmed by directly monitoring the dark decay dynamics at specific probe wavelengths, as shown in Fig. 7(b), in which the decay time constant τ is estimated as the time for the UV-light-induced absorption changes decaying to its e^{-1} of the initial value at $t = 0$. Figure 7(c) shows a typical temporal dark decay dynamics of the UV-light-induced absorption change probed at 400 nm for CMg5 at room temperature. One sees that the

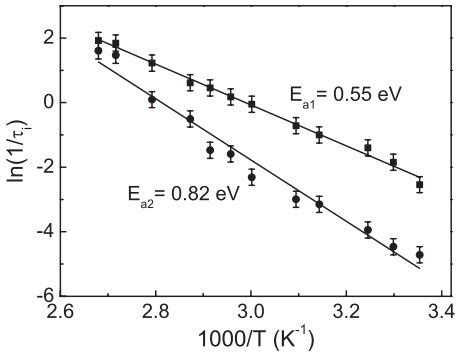

FIG. 8. The temperature dependence of the dark decay time constants τ_1 and τ_2 of the UV-light-induced small hole polarons (O^--V_{Li}) and (O^--$Mg_{Nb}{}^{2+}$), respectively, for CMg5. According to the Arrhenius law, the thermal activation energy E_{ai} was measured to be 0.55 and 0.82 eV for the small hole polarons (O^--V_{Li}) and (O^--$Mg_{Nb}{}^{2+}$), respectively.

dark decay dynamics can be well described by the sum of two stretched exponential decays:[28]

$$\Delta\alpha_{li}(t) = \sum_{i=1,2} \Delta\alpha_{i0}\exp[-(t/\tau_i)^{\beta_i}], \qquad (6)$$

where $\Delta\alpha_{i0}$, τ_i, and β_i $(i = 1,2)$ are the initial absorption change at $t = 0$, the dark decay time constant, and the stretched exponent for the respective small hole polarons. The stretched exponential parameters are fitted to be $\beta_1 = 0.68$, $\tau_1 = 12.7$ s for (O^--V_{Li}), and $\beta_2 = 0.72$, $\tau_2 = 111.6$ s for (O^--$Mg_{Nb}{}^{2+}$), respectively, and the gray curve in Fig. 7(c) shows the fitting result. Good agreement is achieved. We would point out that a sum of two exponential functions cannot give a satisfactory fitting. By measuring the temperature dependence of the dark decay time constant τ_i $(i = 1,2)$ of the respective UV-light-induced small hole polarons, the thermal activation energy E_{ai} $(i = 1,2)$ was measured to be 0.55 and 0.82 eV for the small hole polarons (O^--V_{Li}) and (O^--$Mg_{Nb}{}^{2+}$), respectively, as shown in Fig. 8. This result provides further support on the hole polaronic features of the UV-light-induced absorption change observed in highly Mg-doped $LiNbO_3$ crystals.[25,28]

Based on the above observations, we may suggest the following schematic diagrams of the band structure for both the lightly and highly doped $LiNbO_3$:Mg crystals, as shown in Fig. 9, where the solid horizontal lines represent the energy levels of various effective defect centers in the band gap, and the dashed horizontal lines depict the position of the effective band edge which moves up and down as the crystal temperature changes. For $LiNbO_3$ crystals, the fundamental optical transition occurs in NbO_6 octahedra,[16,20] and the deformation induced by the negatively charged defect centers V_{Li} and $Mg_{Nb}{}^{2+}$ on the oxygen octahedron may generate defect clusters (O^{2-}-V_{Li}) and (O^{2-}-$Mg_{Nb}{}^{2+}$), which might result in deep-level defect centers with the energy levels close to the valence band in the band gap of $LiNbO_3$. This may also be inferred from the reports of Li *et al.*[17] in which the effective band edge of $LiNbO_3$, defined as the photon energy at $\alpha = 15$ or 20 cm^{-1}, is experimentally confirmed to be related to the Li-site vacancy. The spectral fingerprint ratio W^2/M was measured to be ~0.02 eV for both deep-level centers (see Fig. 5), indicating that they are not of the small hole polaronic

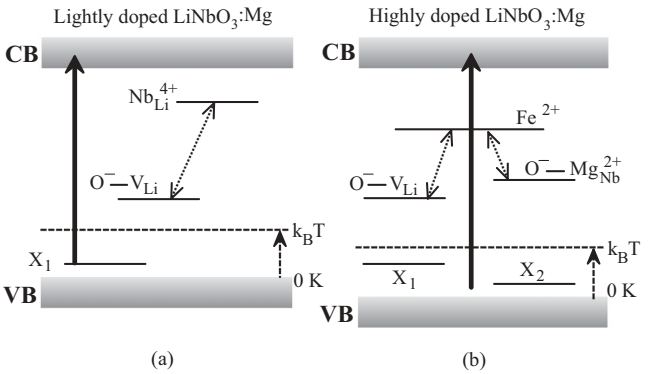

FIG. 9. Schematic diagrams of the band structure and energy levels of various effective defect centers in the lightly (a) and highly (b) doped $LiNbO_3$:Mg crystals, respectively. Here CB and VB represent the conduction and valence bands, respectively. The dashed up arrows indicate the spectral shift of the absorption edge as the crystal temperature increases. The thick solid up arrows represent the photoexcitation by the ultraviolet pump beams such as a 325-nm pump beam, and the dotted double arrows indicate the electron-hole recombination processes between $Nb_{Li}{}^{4+}$ and (O^--V_{Li}), Fe^{2+} and (O^--V_{Li}), and Fe^{2+} and (O^--$Mg_{Nb}{}^{2+}$), respectively.

type.[25] However, for a decisive identification of the deep-level defect centers related to the spectra in Fig. 5, more elaborate experiments are necessary. For the sake of cautiousness and convenience, we may mark, respectively, the deep-level defect center in lightly doped $LiNbO_3$:Mg as X_1 and the additional deep-level defect center in highly doped $LiNbO_3$:Mg as X_2, which increases with increasing Mg-doping concentration, as can be inferred from Fig. 4. Note that the effective band edge of the crystal will be redshifted with the increase of the crystal temperature, and the broad featureless Urbach tail will overlap the absorption band of X_1 and X_2 in both the lightly and highly doped $LiNbO_3$:Mg crystals. Therefore, the absorption spectra near the band edge are characterized by the broad featureless Urbach tail for all samples at high temperatures. At low temperatures, the absorption bands of $X_1$and X_2 appear because the band edge shifts toward high energy significantly and is much deeper in the UV than the absorption bands of $X_1$and X_2, as shown in Fig. 3.

Under the illumination of a 325-nm pump beam at room temperature, electrons are excited either directly from the valence band or from X_1 and X_2 centers, and small hole polarons O^- can be generated in both the lightly and highly doped $LiNbO_3$:Mg crystals. The generation of O^- polarons, both near the V_{Li} and $Mg_{Nb}{}^{2+}$ centers, would induce a broadband UV-light-induced absorption change $\Delta\alpha_{li}$ in the visible and UV spectral ranges in the highly doped $LiNbO_3$:Mg crystals, as shown in Fig. 6. The small hole polarons may recombine with the electrons trapped at the unintentional impurity Fe^{2+}. Such a recombination process can be inferred from the dark decay dynamics of the UV-light-induced absorption changes shown in Fig. 7(a), where there is always some residual UV-light-induced absorption changes in the spectral range around 2.5 eV, which decays at the same rate as that of the small hole polarons (O^--$Mg_{Nb}{}^{2+}$) spectrally peaked at 3.45 eV. However, due to a quick recombination with the

electron small polarons Nb_{Li}^{4+} or electron free small polarons Nb_{Nb}^{4+},[8,24,27–29] a low available UV-pump intensity, and the limited detecting sensitivity of our detecting system, we cannot observe the UV-light-induced absorption change due to the formation of small hole polarons, mainly the O^{-}-V_{Li} polarons, in lightly doped $LiNbO_3$:Mg. Note that the light-induced defect centers, the dark decay dynamics, and the related charge transport processes in our case are quite different from those reported in Ref. 29, in which ultrafast dynamic processes in the time scale of the order of microseconds or milliseconds that are mainly related to electron small polarons Nb_{Li}^{4+} and electron free small polarons Nb_{Nb}^{4+}, spectrally peaked at ∼1.6 and ∼1.0 eV, respectively, were studied in detail. In our case, the dynamic processes are characterized by a time scale of the order of tens of seconds, which are mainly related to the small hole polarons O^{-}, as shown in Fig. 7.

In summary, we have observed the threshold reduction of the Einstein oscillator and the electron-phonon interaction in highly doped $LiNbO_3$:Mg, which could be regarded as the microscopic origin of the significant threshold increase in the photoconductivity and therefore the dramatic suppression of the optical damage in the visible in highly doped $LiNbO_3$:Mg crystals. In addition, a new broad absorption band close to the band edge of $LiNbO_3$ crystals has been observed at cryogenic temperatures, which may be related to the defect clusters O^{2-}-V_{Li} and O^{2-}-Mg_{Nb}^{2+}. Moreover, different types of small hole polarons, O^{-}-V_{Li} and O^{-}-Mg_{Nb}^{2+}, have been confirmed in highly doped $LiNbO_3$:Mg. These defect centers may determine the band-edge optical properties of $LiNbO_3$. It is evident that the concentration threshold behavior of the Einstein oscillator and the electron-phonon interaction will also have important effects on other properties such as the electron and thermal transport processes in $LiNbO_3$:Mg crystals.

ACKNOWLEDGMENTS

This project is supported by the 973 programs (2013CB328702, 2011CB922003, and 2010CB934101), the NSFC (90922030, 11174153, and 10904077), and the 111 project (B07013).

*zhanggq@nankai.edu.cn

[1] T. Volk and M. Wöhlecke, *Lithium Niobate: Defects, Photorefraction and Ferroelectric Switching* (Springer-Verlag, Berlin, 2008).
[2] G.-G. Zhong, J. Jin, and Z.-K. Wu, J. Opt. Soc. Am. **70**, 631 (1980).
[3] D. A. Bryan, R. Gerson, and H. E. Tomaschke, Appl. Phys. Lett. **44**, 847 (1984).
[4] O. F. Schirmer, O. Thiemann, and M. Wöhlecke, J. Phys. Chem. Solids **52**, 185 (1991).
[5] K. Buse, Appl. Phys. B **64**, 391 (1997).
[6] J. Xu, G. Zhang, F. Li, X. Zhang, Q. Sun, S. Liu, F. Song, Y. Kong, X. Chen, H. Qiao, J. Yao, and L. Zhao, Opt. Lett. **25**, 129 (2000).
[7] H. Qiao, J. Xu, G. Zhang, X. Zhang, Q. Sun, and G. Zhang, Phys. Rev. B **70**, 094101 (2004).
[8] G. Zhang and Y. Tomita, J. Appl. Phys. **91**, 4177 (2002).
[9] C. Kittel, *Introduction to Solid State Physics*, 6th ed. (Wiley, New York, 1986).
[10] I. Földvári, K. Polgár, R. Voszka, and R. N. Balasanyan, Cryst. Res. Technol. **19**, 1659 (1984).
[11] G. I. Malovichko, V. G. Grachev, E. P. Kokanyan, O. F. Schirmer, K. Betzler, B. Gather, F. Jermann, S. Klauer, U. Schlarb, and M. Wöhlecke, Appl. Phys. A **56**, 103 (1993).
[12] M. Wöhlecke, G. Corradi, and K. Betzler, Appl. Phys. B **63**, 323 (1996).
[13] L. Viña, S. Logothetidis, and M. Cardona, Phys. Rev. B **30**, 1979 (1984).
[14] F. Urbach, Phys. Rev. **92**, 1324 (1953).
[15] F. Moser and F. Urbach, Phys. Rev. **102**, 1519 (1956).
[16] D. Redfield and W. J. Burke, J. Appl. Phys. **45**, 4566 (1974).
[17] X. Li, Y. Kong, H. Liu, L. Sun, J. Xu, S. Chen, L. Zhang, Z. Huang, S. Liu, and G. Zhang, Solid State Commun. **141**, 113 (2007).
[18] G. D. Cody, T. Tiedje, B. Abeles, B. Brooks, and Y. Goldstein, Phys. Rev. Lett. **47**, 1480 (1981).
[19] B. Abay, H. S. Göder, H. Efeoğlu, and Y. K. Yoğurtcu, J. Phys. D: Appl. Phys. **32**, 2942 (1999).
[20] A. H. Kahn and A. J. Leyendecker, Phys. Rev. **135**, A1321 (1964).
[21] J. D. Dow and D. Redfield, Phys. Rev. B **5**, 594 (1972).
[22] Y. Repelin, E. Husson, F. Bennani, and C. Proust, J. Phys. Chem. Solids **60**, 819 (1999).
[23] N. Iyi, K. Kitamura, Y. Yajima, and S. Kimura, J. Solid State Chem. **118**, 148 (1995).
[24] O. F. Schirmer and D. von der Linde, Appl. Phys. Lett. **33**, 35 (1978).
[25] O. F. Schirmer, J. Phys.: Condens. Matter **18**, R667 (2006).
[26] I. Zaritskii, L. Rakitina, G. Corradi, K. Polgár, and A. Bugai, J. Phys.: Condens. Matter **3**, 8457 (1991).
[27] O. F. Schirmer, M. Imlau, C. Merschjann, and B. Schoke, J. Phys.: Condens. Matter **21**, 123201 (2009).
[28] P. Herth, T. Granzow, D. Schaniel, T. Woike, M. Imlau, and E. Krätzig, Phys. Rev. Lett. **95**, 067404 (2005).
[29] D. Conradi, C. Merschjann, B. Schoke, M. Imlau, G. Corradi, and K. Polgár, Phys. Status Solidi (RRL) **2**, 284 (2008).